Pressure sensitive adhesive blend films for low tack applications

Peter Müller-Buschbaum(*), Thilo Ittner, Edith Maurer,

Volker Körstgens, Winfried Petry

TU München, Physik-Department, LS E13

, James-Franck-Str.1, 85747 Garching (Germany)

Phone: +498928912451, Fax: +498928912473

email: muellerb@ph.tum.de

Keywords

thin films, blends, small-angle X-ray scattering (SAXS), adhesives

Abstract

Polymer blend films consisting of a tacky and a non-adhesive component are promising candidates for low tack applications. Immiscibility of both components results in a phase separation process yielding a tacky matrix with glassy objects embedded. The influence of the blending ratio of the components poly-n-butylacrylate (PnBA) and polystyrene (PS) is addressed. The mechanical information resulting from the tack test shows the possibility to vary the bonding strength of the PSA blend over a wide range. The macroscopic and microscopic structural characterization with optical microscopy and ultra small angle X-ray scattering shows that the blend PnBA:PS exhibits similarities to common filler systems as well as deviates regarding installed structures. Due to the large domain size on a microscopic level, only the tacky component, PnBA, defines the adhesive behavior. The non-adhesive component limits the contact area between the adhesive and the substrate.

Introduction

Pressure sensitive adhesives (PSA) mark one class of adhesives which is characterized by the presence of re-openable bonds. Typical PSA applications from daily life are stick-on notes, scotch tape, labels and re-usable packages. Thus PSA offer the opportunity to connect extremely different materials such as paper, metals, glasses, ceramics and polymers in a re-useable way. The adhesive properties of PSA strongly depend on the way the bonding was created. Typical parameters to quantify this history of bond formation are the applied pressure and the time it was applied. De-bonding becomes possible by applying a distinct force. Typically the performance of PSA is measured in different probe test geometries like the peel or tack test [1-10].

A special class of PSA applications strengthens the idea of an easy de-bonding. These low tack materials, e.g. masking tapes, are commonly used to avoid damage of the material the PSA is bonded with by requiring only very small forces for the de-bonding. In other

applications low-adhesion provides the possibility to position or relocate the adhesive product.

One way of achieving such a characteristic behavior is the addition of a non-tacky component in order to limit the contact area between the PSA system and the bonded surface. For example inorganic solid particles like glass beads or calcium carbonate are distributed over [11-13] the surface of the PSA or dispersed throughout the volume of the PSA. Within the present investigation we follow the idea of mixing tacky and non-adhesive components to reduce the force necessary for the de-bonding. Instead of using inorganic filler materials a second polymer is blended. Blending of incompatible polymers adds the possibility to create marked structures in the mixed film [14-17]. Thus our model system consists of a tacky polymer component, typically characterized by a glass transition temperature below room temperature, and a second glassy polymer component, with a glass transition temperature significantly above room temperature. In more detail, our model system comprises of two blended homopolymers. The one, poly-n-butylacrylate (PnBA), promotes adhesion. The second, polystyrene (PS), increases cohesion and yields structured films, due to the incompatibility with PnBA. The tacky component, PnBA, was used in several investigations in the past [8, 18-20]. The non-adhesive component, PS, was chosen as a standard polymer with well characterized physical parameters, including the polymer-polymer interaction parameter with PnBA, which characterizes the incompatibility. In the blend system PnBA:PS the majority component forms a matrix embedding the minority component [18]. Thus the blend PnBA:PS seems to be a promising candidate with respect to the desired low tack application.

The presented investigation comprises a mechanical characterization based on the tack test and a structural characterization addressing macroscopic and microscopic structures of the blend. In our experimental realization of the mechanic test, a rigid, flat-ended cylindrical punch with a radius a is in contact with the thin PSA film of thickness h. From our experimental parameters a confinement ratio $h/a \sim 1/100$ results. Macroscopic structures are probed with optical microscopy and microscopic structures with x-ray scattering.

The article is structured as follows: The introduction is followed by an experimental sec-

tion describing the sample preparation and the techniques used. The section results and discussion is divided in a mechanical and structural characterization part and followed by a conclusion.

Experimental Part

Sample Preparation: The blended homopolymers are poly-n-butylacrylate (PnBA) with a molecular weight M_w= 260k (M_w/M_n= 3.78) and polystyrene (PS) with M_w= 207k (M_w/M_n= 1.02), respectively. Both components were blended in toluene solution at different weight ratios of PnBA:PS= 9.9:0.1 to 1:9. Adhesive films were prepared with solution casting of the toluene solution with the desired blend ratio onto pre-cleaned glass substrates at ambient conditions. The chosen surface cleaning uses ultra-sonic baths of highly purified water, isopropanol, acetone and toluene which were applied in several subsequent cycles. Varying the solution concentration as well as the amount of solution deposited on the solid support enables the installation of different polymer film thicknesses. For the results presented within this article a thickness of 25 μm was chosen. The polymer-polymer interaction parameter of PnBA and PS is 0.162 at 20^{o}C [21]. Due to this immiscibility between both homopolymers, marked structures result from phase separation.

Tack experiments: Probe tack experiments were performed with a special-designed probe tester allowing the simultaneous observation of the de-bonding process with several other techniques. Fig. 1 shows a sketch of the tack set-up. The developed design is optimized for the use at large scale facilities to allow scattering experiments with synchrotron radiation. Force and distance are measured separately. The maximum velocity is 12.5 mm/s. From underneath, through the transparent glass substrate, the area of contact as well as the macroscopic structures created during the de-bonding are observed with optical microscopy. From the side an x-ray beam can pass through the contact area between PSA and probe and thereby the microscopic structure is accessible. In-situ to both, the

optical as well as the scattering experiment, force-distance curves are measured. Steel as well as glass punches were operated in the probe test. In advance of each tack experiment the punch was cleaned with the same solvent cycle as described above. Typically the diameter of the punch was 2 mm. The surface of the rigid, flat-ended cylindrical punch was characterized by optical microcopy as well as atomic force microcopy (AFM). A mean surface roughness of 1 nm for the glass was determined with AFM on a scan range of 20*20 μm^2.

Fig. 2 shows the three characteristic steps of the tack experiment: a) Approach of the punch, b) contact of film and punch for a fixed time t_o maintaining a fixed force F_o and c) retraction of the punch with velocity v_o. All tack experiments were performed with a parameter set $F_o = 1.85 \pm 0.06$ N, t_o=10 s, $v_o = 1050$ μm/s at a temperature $T = 21^o$C. The obtained force-distance curves typically exhibit a force maximum followed by a force plateau as shown in fig. 2d).

Optical investigation: The sample surfaces were observed with optical microscopy using a Zeiss Axiotech 25H optical microscope with magnifications between 4 times and 100 times. A Hitachi KP-D50 CCD camera recorded the micrographs.

X-ray scattering experiments: Ultra small angle X-ray scattering (USAXS) was measured at the BW4 beamline at the synchrotron HASYLAB (DESY, Hamburg). The selected wavelength was λ =0.138 nm. The probe tester was placed horizontally on a two-circle goniometer with a y,z-translation table to align the beam with respect to the desired position. Whereas the probe tester was operated in air, the remaining parts towards the source and the detector were under high vacuum conditions. The beam quality was optimized by using a set-up of high quality entrance cross-slits. For further details concerning the beamline see ref. [22]. In the USAXS experiment due to the large sample-detector distance of 12.7 m structures between 20 and 400 nm are resolvable. Thus structures are addressed which are not visible with optical methods. The scattered signal was recorded with a two dimensional detector which consists of a 512x512 pixel

array. Due to the tack probe geometry which can be regarded as a small horizontally placed slit the scattering pattern is strongly anisotropic. Scattering parallel to the force applied in the axis-symmetric probe geometry (along the cylinder punch axis) is mainly due to reflections on the PSA and the probe surface and thus not further evaluated in this investigation. Scattering in the perpendicular direction, however, results from structures between the PSA and the probe. Consequently, from the two dimensional scattering picture horizontal slices with respect to the PSA film surface were cut. For an improvement of the statistics the intensity was integrated in vertical direction ($\Delta q_{=} \pm 2.57 \cdot 10^{-3}$ nm^{-1}).

Results and Discussion

The mechanical characteristics are determined by performing probe-tack experiments. For fixed key parameters such as contact pressure, contact time, de-bonding velocity and PSA film thickness, the influence of the blend ratio PnBA:PS is addressed. The macroscopic structure is probed with optical microscopy and the microscopic structure is determined by ultra small angle X-ray scattering (USAXS) experiments in-situ during the de-bonding process.

1. Mechanical characterization:

The parameters we applied in the tack test are motivated by typical boundary conditions resulting from low tack applications. So contact pressure, contact time and de-bonding velocity reflect the common way of bonding and de-bonding low tack tapes.

Not depending on the blending ratio, the force-distance curves probed with the tack test show one characteristic shape illustrated in fig.2d. A peak, yielding the maximum force necessary to start the de-bonding, is followed by a force plateau resulting from the presence of fibrils. This shape of the force-distance curve is typical for the tacky component (PnBA) of the investigated blend [8, 18-20]. Already the addition of a few percent PS results in a clear decrease of the maximum force. 10% of PS are sufficient

to reduce the maximum force to approximately one fourth of the reference value of pure PnBA [18-20]. At 40 and 50 % of PS the remaining force is that small, that it is hardly detectable in the standard tack set-up. Therefore a high sensitivity set-up was applied, which is however not within the main focus of this article. Fig. 3 shows the behavior of the maximum force. Typically 10 to 20 individual tack experiments were statistically analyzed. The shown error bars basically reflect the dependence of the measured values from the actual position on the blend film surface. The maximum force (and the total energy) necessary to open the adhesive joint decreases in a non linear dependence with increasing weight fraction ϕ_{PS} of the blend component PS. Therefore, the addition of PS turns out to be a very effective possibility to tune the tackiness of the PSA system.
Whereas Fig. 3 is well suited to design low tack applications, for an improved understanding of the underlying process a structural characterization has been performed.

2. Structural characterization:

a) Macroscopic structures: As well known from other blend systems [14-17] due to the immiscibility of both components, PnBA and PS, a marked structure results from a phase separation process. Recent scanning probe experiments utilizing pulsed force mode on thin PnBA:PS blend films determined the chemical composition and the surface structure due to the related mechanical differences [21]. The majority component forms a matrix embedding the minority component as disperse objects. The size of these objects decreases with decreasing amount of the minority component. Up to a blending ratio of 5:5 PnBA forms a tacky matrix with rigid PS islands inside. As a consequence, we restricted our mechanical tack experiments to films with a majority of PnBA as compared to PS, including the symmetric blend with PnBA:PS= 5:5.
However, for PSA applications thick blend films are required instead of thin films. Following scaling laws established for polymer blend films, the phase separation structures coarse with the film thickness [23, 24]. Therefore, optical microscopy is sufficient to access such phase separation structures. Fig. 4 shows representative optical micrographs

picturing these structures. From different magnifications used in this investigation, one fixed magnification is selected, which allows to show the strong change in structure size. From the series of different blending ratios five examples are picked to demonstrate the changes in the structural size, given by the lateral extension of the surface features, as well as of the type of morphology.

With optical microscopy mainly the surface structures are visualized. Due to phase separation the bulk structure of the film is also non homogeneous. Along the idea of a filler material, the bulk morphology is analogue and consists of minor polymer domains embedded in the major polymer matrix (PS domains in a PnBA matrix). However, compared to simple filler material such as spherical glass beads, the created glassy inclusions are of more complex shape. As visible in Fig. 4 the shape deviates strongly from a sphere.

To enable a further understanding, a statistical treatment of the optical images has been applied. From the optical micrographs, the two-dimensional Fourier transform is calculated using a two-dimensional fast Fourier algorithm (FFT). Because the preparation technique does not introduce a preferential orientation of the structures, the Fourier transform exhibit radial symmetry (see Fig. 4f) and statistics are improved by applying a radial average [17]. Radial averaged data from various micrographs measured with different magnification of one sample are combined into one master curve [23-25] to enlarge the range of reciprocal lengths in comparison to the individual data of one magnification. Nevertheless, the Fourier transformation of optical micrographs relies on the assumption that different colors (or gray values) result from different sample heights [25]. As a consequence, the obtainable intensity versus reciprocal length data are not directly the power spectral density function of the height-height correlation function. However, this does not effect the possibility to detect the most prominent in-plane length from the position of the maximum in intensity in reciprocal space.

The most prominent in-plane length enables a statistical characterization of the introduced surface structure. In Fig. 5 the most prominent in-plane length detected from this procedure replaces the weight fraction of the PS component used in Fig. 3. Moreover, the maximum force during de-bonding depends on the contact area $A_{contact}$ between the

adhesive and the probe. Within the idea, that PS acts only as an inert filler, which reduces the effective tacky surface area, the contact area differs for different amounts of PS. The more PS the blend film contains, the less macroscopic contact area is observed (by the optical microscope from underneath the substrate). Therefore in Fig. 5 the maximum stress $\sigma_{max} = F_{max}/A_{contact}$ replace the maximum force used in Fig. 3.

By normalization the resulting value σ_{max} should be independent of the lateral length Λ. However, as plotted in Fig. 5, σ_{max} decreases with increasing value of Λ in a non-simple way. In a double logarithmic plot the data suggest the presence of two different regimes with two different power laws $\sigma_{max} \sim \Lambda^{\alpha}$. For small lateral length $\Lambda < \Lambda_c$ an exponent $\alpha = -6$ fits the data and for large lateral lengths $\Lambda > \Lambda_c$ a smaller exponent $\alpha = -3/5$ is fitted. For the present system, Λ_c has a value of 3.2 μm. We might attribute an additional stiffness of the blend films resulting from the bulky inclusions to be responsible for the observed $\sigma_{max}(\Lambda)$ dependence. Moreover, two additional mechanisms will deserve consideration:

i) The additional trapping of air due to the presence of non tacky regimes: The lateral length Λ plotted in Fig. 5 has to be identified with the diameter of the rigid and non tacky PS domains shown in Fig. 4. Due to the spatial arrangement of the PS domains, several of them are embedded in the contact area defined by the punch diameter. As mentioned, no effective tacky contact is formed and thus the trapped air is collected within these domains. As a consequence, during the bond state there are already cavities existing inside the contact area. These initial cavities can grow under load similar to the growth of the typically emerging cavities. In contrast, in pure PnBA due to the full contact, with optical microscopy no regions of trapped air can be observed [8, 18-20].

ii) The spatial restriction of the lateral cavity growth due to the presence of non tacky regimes: The homogeneous expansion of the contact area under traction is followed by cavitation and the lateral growth of once initiated cavities. In pure PnBA the cavities can grow until neighboring cavities meet. Having non tacky PS domains embedded in the contact area introduces cavities, which prevent the undisturbed lateral cavity growth.

In addition, during the later stages of de-bonding, characterized by the presence of fibrils

connecting PSA and probe (denoted vertically expanded state), the flow of PnBA during traction might be disturbed. Embedding glassy and stiff PS domains inside the PnBA matrix suppresses the lateral flow. Therefore, the microscopic structure might be effected by the blending of PnBA with PS as well.

b) Microscopic structures: Whereas macroscopic structures in the blend PSA deviate from standard filler systems and cause a more complex macroscopic behavior, its effect on the microscopic structure is revealed with x-ray scattering.

In-situ during the de-bonding with USAXS information is detected on length scales, which is not accessible with optical methods [20, 26]. Due to the necessity to perform these experiments at a synchrotron and the limited synchrotron beamtime available in general, we concentrate on two blending ratios. We selected PnBA:PS= 9:1 and 7:3 to cover a regime which is well within the regime having a well defined force curve with a force maximum present as well as having a certain amount of non tacky homopolymer added. As visible in Fig. 4a and b the surface structures are well characterized by rigid, circular PS domains embedded in a PnBA matrix.

To address structures in the vertically expanded state, the USAXS measurements were performed at quantized distances during the de-bonding. To optimize between the time which is necessary to do the mechanical test and the available flux at the synchrotron each 125 μm (between the probe and the PSA surface) a scattering pattern was collected without averaging over distances in-between. Fig. 6a shows a sketch of the applied scattering geometry. The beam (400 μm diameter) is solidly attached to the initial PSA surface. As a consequence, with increasing punch-probe distance the illuminated volume is not constant. In transmission geometry the scattered intensity was recorded with a two dimensional detector. Fig. 6b and c show two examples of two dimensional intensity distributions. In Fig. 6b the scattering experiment was performed without having a PSA film present. The bare probe was pressed on the bare glass substrate and moved up again. At a fixed distance of 250 μm, the measured signal comprises of two vertical intensity streaks (in α_I direction). Both streaks are aligned parallel to the applied force and result

from the reflection of the x-ray beam from the probe and from the substrate surface. In Fig. 6c the scattering experiment was performed with the PSA blend film present. After performing the tack test (as described in the experimental section) at a fixed distance of 250 μm, the measured signal differs. Most striking are the horizontal intensity streaks (in α_{II} direction) due to the scattering from the vertically expanded PSA film. In addition, the vertical intensity streaks are changed slightly as well. As explained in the experimental section, the analysis is restricted to horizontal cuts, carrying the transmission signal, because the vertical cuts show a simple decay of the intensity only.

Fig. 7a and b show these horizontal cuts from the 2D scattering data for distances between 125 and 1000 μm. With increasing punch-probe distance the data are successively shifted along the y-axis for clarity. The two selected blend compositions of PnBA:PS= 9:1 and 7:3 are shown, respectively. We restrict to a range of scattering vectors q_y, which focusses on the shape of possible nano-objects. In general, both series of data look very similar with respect to the major features. Of course there are small differences in detail, however, the strong similarity allows for one general description of the measured features, irrespectively of the exact blend ratio.

Before contact no intensity is scattered in the horizontal direction. Right after the onset of de-bonding in the vertically expanded regime a marked feature in the scattering signal is observed. This feature is a direct proof of the presence of a sub-structure well resolvable with x-rays. It can be described as a broad peak close to the position $q_y \sim 0.07$ nm^{-1}. With increasing distance between punch and PSA surface the intensity of the broad peak decreases, whereas its position remains constant. Above 750 μm (two topmost curves in Fig. 7) the broad peak disappears.

To work out numbers, the USAXS data are modelled with a model assuming cylindrically shaped nano-bubbles, which was successfully applied for the explanation of the USAXS data measured at pure PnBA [20]. Fig. 8 sketches the applied model. With optical techniques only the well known large cavities are visible (see Fig. 8a). Due to the reflection of light from the punch surface, the cavities appear in white and the polygonal polymer structure separating the cavities in black. The untouched PSA film surface appears in

white as well. With increasing amount of PS added to the blend, in these transmission micrographs the phase separation structures yield lateral fluctuations of the refractive index. Due to the low magnification the lateral phase separation structures are not resolved and as a consequence the pure PSA film only appears less white. However, the tacked surface area is strongly modified from the presence of the cavities and in addition easily detected from the presence of a circularly shaped rim of polymer separating both, untouched film and tacked film.

In more detail, our model consists of four contributions which give rise to the USAXS signal observed. The 2D intensity data suggest the presence of rotational symmetric objects such as spheres or cylinders. Basically the nano-bubbles are considered as cylinders of radius r which appear in the schematic sketch shown in Fig. 8b as small circles. The cylinders are oriented with the long axis parallel to the force applied in the tack test. Due to the absence of any modulations in the vertical intensity streaks, the height of the cylinders is not resolved (larger than 400 nm). Moreover, due to the absence of modulations in the vertical intensity streaks, a spherical object shape can be excluded, although energetic considerations might favor spheres. Thus the cylindrical nano-bubbles give rise to a form factor contribution [27]

$$P(q) = \int_0^\infty \left(\frac{J_1(qr)}{qr} \right)^2 r^4 f_r(r)\, dr \tag{1}$$

with a log-normal distribution for the radius r with a mean value ξ_1 and a width σ_r [28]

$$f_r(r) = \exp\left(-\frac{(\ln r - \ln \xi_1)^2}{2\sigma_r^2} \right) \quad . \tag{2}$$

Here $J_1(x)$ denotes the Bessel function of first order and first kind. The arrangement of the individual nano-bubbles is described by one dimensional structure factor [29, 30]

$$S(q) = \frac{1 - \exp(-2q^2\sigma_D^2)}{1 - 2\exp(-2q^2\sigma_D^2)\cos(q\xi_2) + \exp(-2q^2\sigma_D^2)} \tag{3}$$

with a characteristic distance ξ_2 between adjacent nano-bubbles and a variance σ_D. In addition the diffuseness of the interfaces was accounted by a fixed roughness contribution on the order of $\sigma_R \sim$4 to 9 nm via

$$I_\sigma(q) = \exp(-q\sigma_R^2) \quad . \tag{4}$$

The overall intensity is considered as the product of these contributions including a q-independent background B [31]

$$I(q) = NP(q)S(q)I_{\sigma}(q) + B \tag{5}$$

The resulting fits are shown with solid lines in Fig. 7.

Consistent with the unchanged position of the broad intensity peak in the scattering data, one key parameter, namely the radius of the nano-bubbles ξ_1 remains constant as a function of the distance between the probe and the PSA surface. Within the error bars, the determined value of $\xi_1 = 95 \pm 5$ nm agrees very well with the values determined in case of the pure PnBA ($\xi_1 = 98 \pm 5$ nm) in a recent investigation [20]. Moreover, within the experimental error, both values are not effected by a variation in the blend composition. Thus the addition of PS does not affect the microscopic structure which is characteristic for the de-bonding process. Along this line, it is tempting to identify this sub-structure as a type of fingerprint of the adhesive component.

The observed size of the nano-bubbles fits well into the regime which is below the critical radius of growth reported in case of other adhesive systems [32, 33]. In case of small sized cavities a certain activation energy barrier needs to be overcome to enable a cavity growth. As the stress increases, this energetic gap decreases. Cavity growth depends on the initial size of the cavities and the available elastic energy. Thus perhaps the nano-bubbles are a precursor of the optically observable macroscopic cavities which form out of some of the nano-bubbles by overcoming the activation energy barrier. Because the available elastic energy is limited, only a fraction of the nano-bubbles are transferred into macroscopic cavities and the rest remains unchanged in size and position. Along this line, the size and shape of the nano-bubbles will depend on the PSA system. Replacing the polymeric PSA yields a change of the sub-structure in agreement with our findings: Cavities in PnBA are cylindrically shaped [20] irrespectively of the amount of non tacky homopolymer added, whereas cavities in P(EHA-co-MMA) are needle like [34].

Due to the technical complexity of the scattering experiment, we have to restrict to the vertically expanded state, which is characterized by the presence of large macroscopic cav-

ities and allows for a separation between punch and film by at least 125 μm. At present, at smaller distances the scattering signal is too weak to enable a doubtless interpretation. The question if the nano-bubbles are present in the earlier stages of the de-bonding process, remains open. As a consequence, the mechanism for cavity formation (widening of already existing air bubbles or gas diffusion through the polymer) cannot be detected.

Because the reduced tack with increased amount of rigid polymer (PS) added is linked with the reduced tacky surface area, in the scattering experiment a reduced number of scattering objects might be expected as well. Due to the variation of the amount of material during retraction we have in principle no access to absolute intensities, which prevents a direct comparison between the scattering data from individual samples. The absolute numbers of nano-objects contributing to the scattered intensity are thus inaccessible. Nevertheless, the observed decrease in the peak intensity within one retraction experiment can be analyzed (see equation 5). To picture the decay and compare between pure PnBA [20] and the two blends with PnBA:PS= 9:1 and 7:3 the normalized number of nano-objects is plotted in Fig. 9. Normalization is performed with respect to the number of nano-objects N_o extracted at the first investigated punch-probe distance of 125 μm and with respect to the illumination L with the x-ray beam.

In general, the normalized number of nano-objects $N/(N_oL)$ reduces with increasing distance for the pure PnBA as well as for the blended PnBA films. In more detail, this decrease depends on the amount of PS added. In pure PnBA more nano-objects are present than in the blend with 10% PS, which again exhibits more nano-objects than in the blend with 30% PS. Thus in the late stages, the data shown in Fig. 9 are consistent with the idea of a decreasing tacky surface area with increasing amount of PS added, which results in a decreased number of nano-bubbles present. However, the type of decay differs between pure PnBA and both blends. This difference can result from the surface structures which were optically observed.

With respect to the aim of low tack materials, the added PS works perfectly comparable to an inert filler on the microscopic scale. Interesting for applications is the absence of the non-tacky component in the vertically expanded material during de-bonding. As a

consequence, the added non-tacky PS is not transferred to the material in contact with the blend PSA. Only the tacky component, PnBA in the presented work, is transferred. Thus the behavior is identical to the pure adhesive system, but with a tailored reduced tack.

Conclusion

Instead of inorganic fillers, an low tack PSA is realized by the addition of a non-adhesive polymer component namely PS to the well investigated model adhesive PnBA. Thereby, the pure homopolymer PSA is transformed into a blend PSA film. Due to the immiscibility of both polymers, marked structures dominate the PSA film. By the blend ratio, the typical size of the non-adhesive objects embedded in the tacky film is tailored. Thus the technique allows to operate with fillers of different size and the contact control is build-in mechanically.

In contrary to typical filler applications, which allow to vary the filler concentration independently from the filler size, in polymer blend systems both parameters are coupled. However, one advantage in applications can be the improved processibility of polymer blend systems compared to filler based systems. At least in solution based applications the mechanics during deposition of the filler based material strongly depend on the filler concentration. In case of polymer blend solutions, a change in the blend ratio does not cause comparable large changes in key parameters such as viscosity.

With respect to the mechanical tack test, only the component PnBA contributes which gives rise to a strong decrease in the stickiness of the blend surface with increasing PS content. This manifests for example in a strong decrease in the maximum force necessary to separate the punch and the PSA film and the desired low tack conditions can be installed.

Advantageous for applications is the absence of a strong influence of the blend ratio on the microscopic sub-structure. In coexistence to the macroscopic cavities, optically inaccessible nano-bubbles are present. The shape and distance between adjacent nano-bubbles

remains constant within the total vertically expanded state. However, the shape strongly differs from recently observed sub-structures in other acrylate based model PSA polymers. Thus obviously the observed sub-structure is a finger print of the tacky component in contact with the punch surface.

Acknowledgment

We thank S. Cunis for her help during setting up the BW4 beamline at the HASYLAB. J. Kraus, C. Lorenz-Haas, B. Mahltig and O. Wunnicke helped during the USAXS experiments. Additionally we owe many thanks to R. Gehrke for his general support of the experiment at HASYLAB. We thank M. Stenert and F. Bandermann for supplying the PnBA and D. Wulff and N. Willenbacher for stimulating discussion. We obtained financial support by the BMBF (Förderkennzeichen 03CO333) and DFG (MU1487/6-1).

Literature

[1] Chan, H.K., Howard, G.J.; *J. Adhesion* **1978**, *9*, 279.

[2] Zosel, A.; *Coll. Polym. Sci.* **1985**, *263*, 541.

[3] Tse, M.F., Jacob, L., *J. Adhes.* **1996**,*56*, 79.

[4] Creton, C. In *Material Science and Technology - Processing of Polymers*; Meijer, H.E.H., Eds.; VCH: Weinheim, 1997, Vol. 18.

[5] Crosby, A.J., Shull, K.R., Lakrout, H., Creton, C.; *J. Appl. Phys.* **2000**, *88*, 2956.

[6] Luzinov, I., Julthongpiput, D., Liebmann-Vinson, A., Cregger, T., Foster, M.D., Tsukruk, V.V.; *Langmuir* **2000**, *16*, 504.

[7] Li, L.H., Macosko, C., Korba, G.L., Pocius, A., Tirrell, M.; *J. Adhesion* **2001**, *77*, 95.

[8] Lakrout, H., Creton, C., Ahn, D., Shull, K.R.; *Macromolecules* **2001**, *34*, 7448.

[9] Goh, L.L.N., Toh, S.L., Chooi, S.Y.M., Tay, T.E.; *J. Adhesion Sci. Technol.* **2002**, *16*, 729.

[10] Moon, S., Foster, M.D.; *Langmuir* **2002**, *18*, 1865.

[11] Erwin, J.V.; US patent 3314838 **1967**.

[12] Reed, D.R.; Stafford, T.W.; US patent 4054697 **1977**.

[13] Ochi, K.; US patent 4556595 **1985**.

[14] Krausch, G.; *Mat. Sci. Eng. Rep* **1995**, *14*, 1.

[15] Geoghegan, M., Krausch, G.; *Prog. Polym. Sci.* **2003** *28*, 261.

[16] Wang, J., Composto, R.J.; *Interf. Sci.* **2003** *11*, 237.

[17] Müller-Buschbaum, P., Bauer, E., Wunnicke, O., Stamm, M.; *J. Phys. Condens. Matter* **2005** *17*, S363.

[18] Zosel, A.; *J. Adhesion Sci. Technol.* **1997**, *11*, 1447.

[19] Zosel, A.; *Int. J. Adhesion and Adhesives* **1998**, *18*, 265.

[20] Müller-Buschbaum, P., Ittner, T., Petry, W.; *Europhys. Lett.* **2004** *66*, 513.

[21] Stenert, M., Doring, A., Bandermann, F.; *e-Polymers* **2004** *15*, 1.

[22] Gehrke, R.; *Rev. Sci. Instrum.* **1992**, *63*, 455.

[23] Müller-Buschbaum ,P., Gutmann, J. S., Stamm, M.; *J. Macromol. Sci. B* **1999** *38*, 577.

[24] Gutmann, J. S., Müller-Buschbaum, P., Stamm, M.; *Farady Disc* **1999** *112*, 285.

[25] Renger, C., Müller-Buschbaum, P., Stamm, M., Hinrichsen, G.; *Macromolecules* **2000** *33*, 8388.

[26] Maurer, E., Loi, S., Wulff, D., Willenbacher, N., Müller-Buschbaum, P.; *Physica B* **2004** *357*, 144.

[27] Lode, U. , Pomper, T., Karl, A., Krosigk, G. von, Cunis, S., Wile, W., Gehrke, R.; *Macromol. Rapid Commun.* **1998**, *19*, 35.

[28] Wadsworth, H. M.; In *Statistical Methods for Engineers and Scientists*, edited by R. W. Hauserman, pp. 6.26-6.29. New York: McGraw-Hill, 1990.

[29] Hosemann, R., Bahgi, S. N.; *Acta. Crystallogr. A* **1952**, *5*, 612.

[30] Vignaud, G., Gibaud, A., Wang, J., Sinha., S., Daillant, J., Grübel, G., Gallot, Y.; *J. Phys. Condes. Matter* **1997**, *9*, L125.

[31] Higgins, J. S., Benoit, H. C.; In *Polymers and Neutron Scattering*, pp. 192-244. New York: Oxford University Press, 1996.

[32] Dollhofer, J.; Chiche, A.; Muralidharan, V.; Creton, C.; Hui, C. Y.; *Inter. J. Solids. Structures* **2004**, *41*, 6111.

[33] Chiche, A.; Dollhofer, J.; Creton, C.; *Euro. Phys. J. E* **2005**, *17*, 389

[34] Maurer, E.; Loi, S.; Müller-Buschbaum, P.: de-bonding of pressure sensitive adhesives: A combined tack and ultra-small angle X-ray scattering study; in "Adhesion - Current Research and Applications", edt. W. Possart, Wiley-VCH, 421-434 (2005)

Figure captions

Figure 1: Schematic a) 3d and b) side view sketch of the used tack apparatus which allows for an in-situ mechanical testing, x-ray scattering and optical investigation. Static components are shown in light gray and moving components in dark gray. The components are 1- motor, 2- distance sensor, 3- force sensor, 4- punch, 5- sample and 6- optical microscope.

Figure 2: Schematic side-view of the three characteristic steps of the tack experiment. a) The flat-ended cylindrical punch approaches from above with a constant velocity v. b) During the contact phase, the punch is pressed onto the PSA film surface with a fixed force F for the desired contact time. c) For the de-bonding of the adhesive joint, the punch is moved up with a constant velocity and the force is measured as a function of the distance between punch and probe. As shown in the sketch, the vertically expanded state is characterized by a fibrillar like connection between punch and probe. d) Typical force-distance curve measured for a blend containing 2 % PS.

Figure 3: Maximum force F_{max} measured in the tack test as a function of the weight fraction ϕ_{PS} of the blend component PS. The solid line is a guide for the eye.

Figure 4: Optical micrographs of the surface of a PnBA:PS blend film with a blending ratio of a) 9:1, b) 7:3, c) 5:5, d) 3:7 and e) 1:9 after preparation. Differences in the gray values result from surface structures of different height, which look white in case they reflect more light. Each micrograph shows a surface size of 200x150 μm^2. f) Example of intensity distribution resulting from the 2d Fourier transformation of an optical micrograph.

Figure 5: Double logarithmic plot of the maximum stress σ_{max} versus the most prominent in-plane length Λ as calculated from the optical micrographs. The solid lines are fits to the data picturing the two step behavior.

Figure 6: a) Schematic picture of the experimental set-up used in the scattering experiment. In case of the first distances between punch and film probed with USAXS, the x-ray beam (coming from the left in this sketch) fully illuminates the vertically expanded film. Example of a typical scattering signals b) without and c) with adhesive material present between the punch and the solid support.

Figure 7: Horizontal cuts from the 2D scattering data measured at different distances between the probe and the PSA surface: $125\mu m(\circ)$, $250\mu m(\triangle)$, $375\mu m(+)$, $500\mu m(\times)$, $625\mu m(\diamond)$, $750\mu m(\star)$, $875\mu m(\blacksquare)$ and $1000\mu m(\bullet)$. The solid lines are fits with the model as explained in the text. The selected blend ratio is a) PnBA:PS= 7:3 and b) 9:1.

Figure 8: a) Optical micrograph picturing the cavitation structure present between punch and PSA film at a position in the plateau of the force-distance curve in case of a PnBA rich blend. The dark areas represent polymeric material surrounding the cavities shown in white. The bar represents a length of 500 μm. A circular shaped rim separates the flat PSA film from the surface area which was in contact with the punch. b) Schematic sketch of a horizontal cut through the polygonal polymer structure surrounding the macroscopic cavities. Due to the high level of magnification the optically invisible nano-bubbles are visible. The differences in the real part of the refractive index as detected with the X-ray scattering are sketched with the chosen gray scale.

Figure 9: Normalized number of nano-objects $N/(N_oL)$ plotted as a function of the punch-probe distance d. The probed number of nano-objects N is normalized by the number of nano-objects N_o present in the first scattering data at a punch-probe distance of 125 μm and by the illumination L with the x-ray beam. Data from this investigation on blends with a ratio PnBA:PS= 9:1 (open circles) and 7:3 (crosses) are compared to data from pure PnBA (dots) from [20]. The solid and dashed lines are guides to the eye to emphasize on the deviations.

Figures

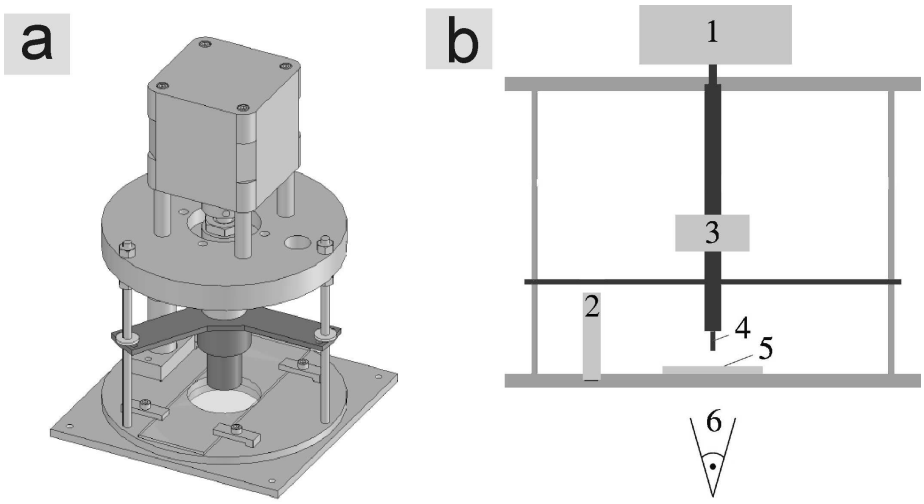

Figure 1:

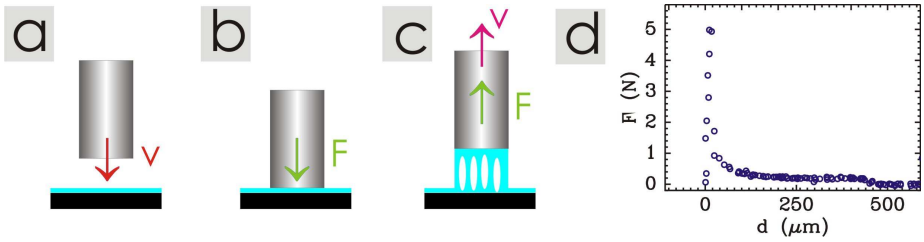

Figure 2:

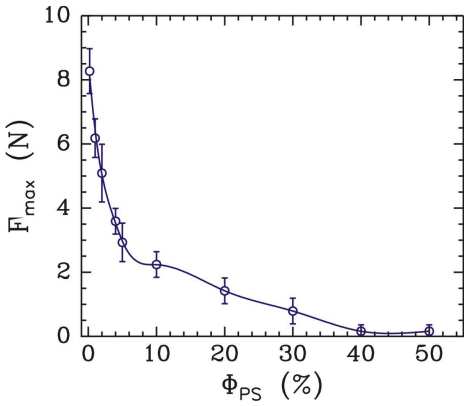

Figure 3:

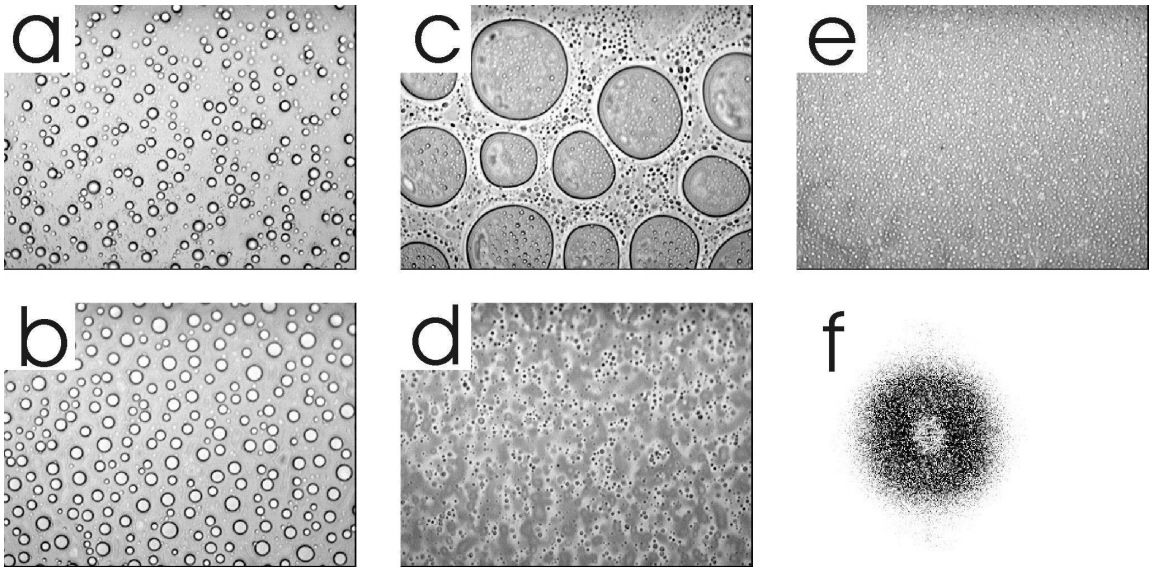

Figure 4:

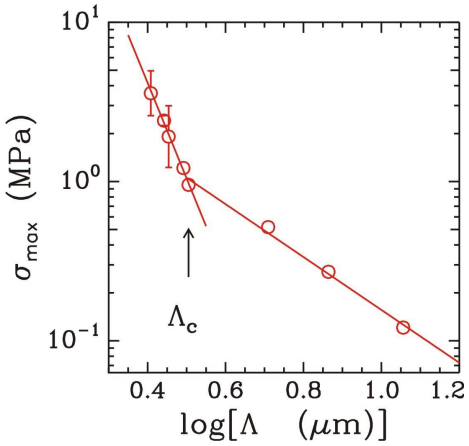

Figure 5:

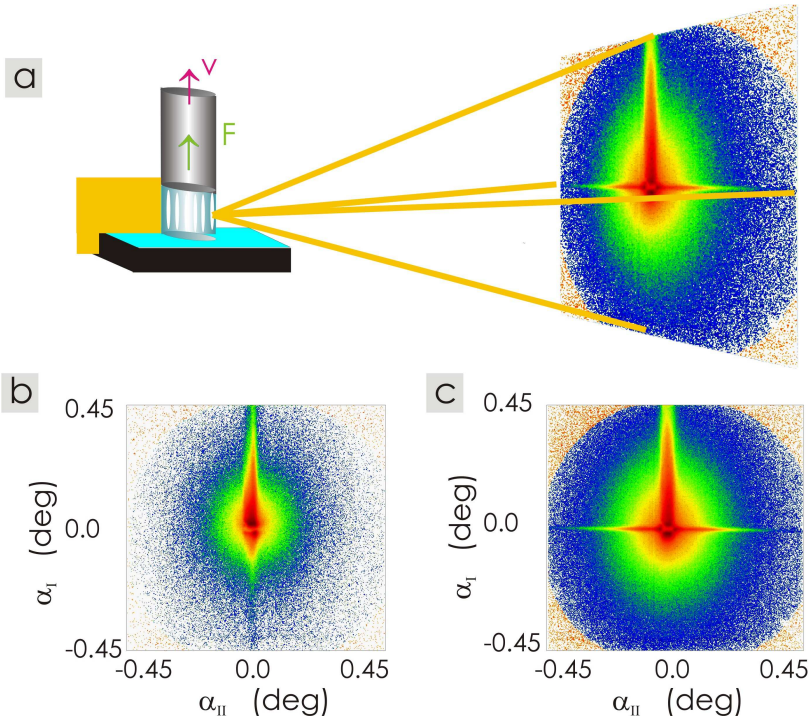

Figure 6:

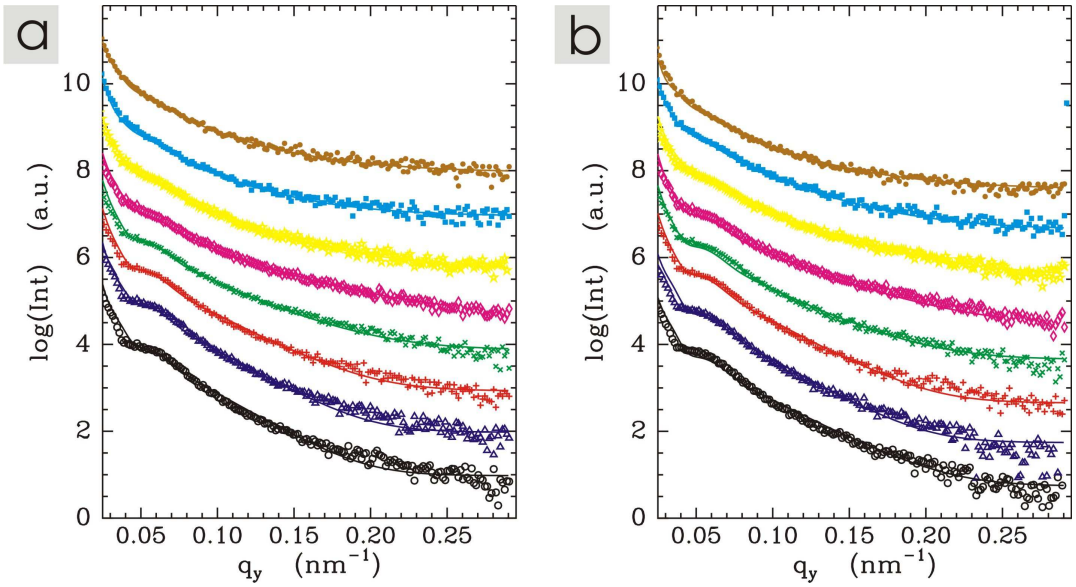

Figure 7:

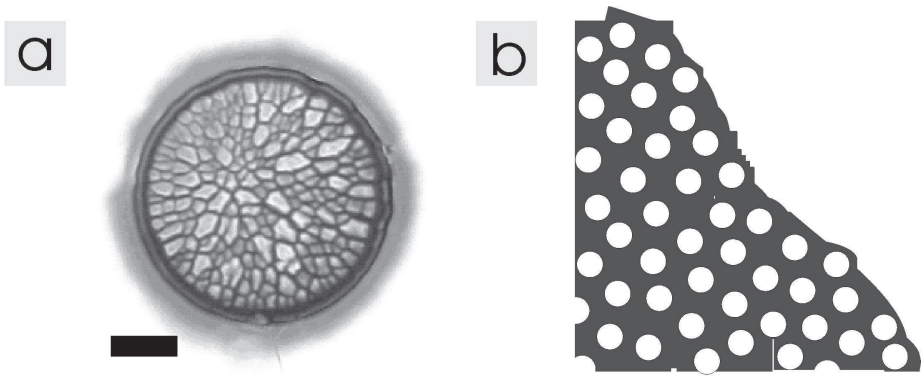

Figure 8:

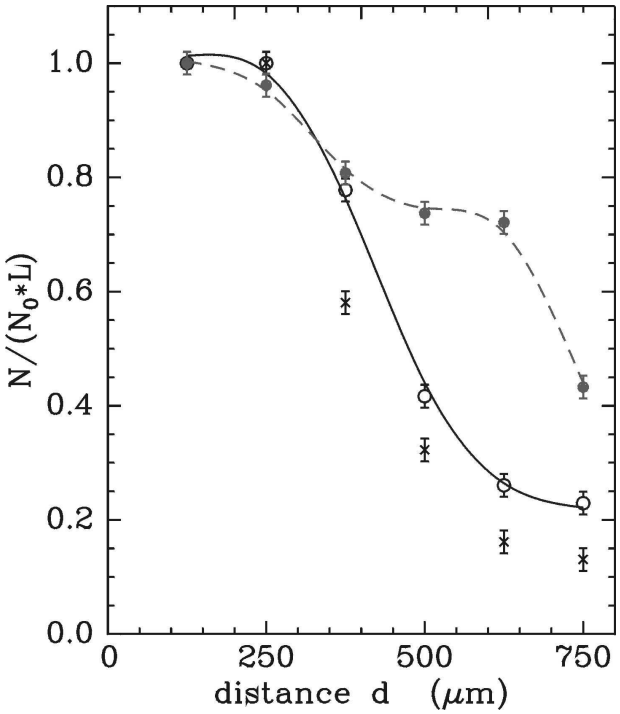

Figure 9:

Text for Table of Contents

Mechanical and structural properties of polymer blend films consisting of a tacky and a non-adhesive component for low tack applications are investigated. The tack test is combined with in-situ ultra small angle x-ray scattering and optical microscopy.

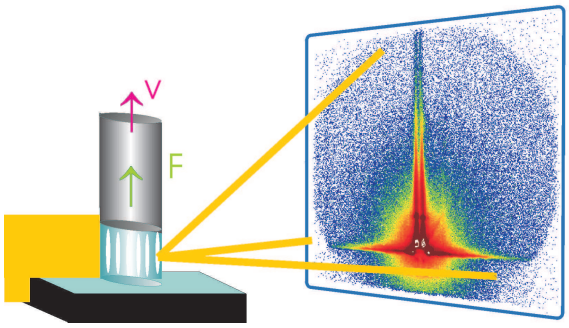

Figure 10: A graphic for the Table of Contents